Amide-I lifetime-limited vibrational energy flow in a one-dimensional lattice of hydrogen-bonded peptide units

Vincent Pouthier*
Institut UTINAM, Université de Franche-Comté, UMR CNRS 6213, 25030 Besançon Cedex, France
(Received 11 July 2008; revised manuscript received 11 September 2008; published 4 December 2008)

A time-convolutionless master equation is established for describing the amide-I vibrational energy flow in a lattice of H-bonded peptide units. The dynamics is addressed within the small polaron formalism to account for the strong coupling between the amide-I vibron and the phonons describing the H-bond vibrations. Therefore, special attention is paid to characterize the influence of the amide-I relaxation on the polaron transport properties. This relaxation is modeled by assuming that each amide-I mode interacts with a bath of intramolecular normal modes whose displacements are strongly localized on the C=O groups. It has been shown that the energy relaxation occurs over a very short time scale which prevents any significant delocalization of the polaron. At biological temperature, the polaron explores a finite region around the excited site whose size is about one or two lattice parameters. However, two regimes occur depending on whether the vibron-phonon coupling is weak or strong. For a weak coupling, the energy propagates coherently along the lattice until the polaron disappears. By contrast, for a strong coupling, a diffusive regime occurs so that the polaron explores a finite size region incoherently. In both cases, the finite polaron lifetime favors the localization of the vibron density whose amplitude decreases exponentially.

DOI: 10.1103/PhysRevE.78.061909 PACS number(s): 87.10.−e, 87.15.−v, 71.38.Ht, 63.22.−m

I. INTRODUCTION

Since the seminal work of Davydov and co-workers [1] on bioenergy transport in proteins, both theoretical and experimental evidences suggest that vibrational energy flow in α helices may result from a polaron mechanism [2–14]. The energy is transferred by amide-I vibrations (C=O stretching modes) which delocalize due to dipole-dipole couplings between peptide units leading to the formation of an exciton called vibron. Since each C=O group is engaged in a H bond, the vibron strongly interacts with the phonons describing the collective dynamics of the H-bond network. Therefore, its creation induces a lattice distortion, i.e., a virtual cloud of phonons, that corresponds to a contraction of the H bonds surrounding the excited site. The vibron dressed by this distortion forms the so-called small polaron.

From a theoretical point of view, the dressing mechanism is accounted by performing a Lang-Firsov transformation [15] which is exact when the dipole-dipole coupling is neglected. However, when the delocalized nature of the vibron is considered, a weak coupling remains between the polaron and the phonons. It is responsible for dissipation and it leads to the incoherent diffusive motion of the polaron. The transport properties of a small polaron coupled with a phonon bath have been extensively studied during the last three decades to characterize exciton-phonon systems [16–24] and polaron and bipolaron in α helices [25,26]. By using a standard projector method [27–29], a generalized master equation (GME) for the polaron reduced density matrix (RDM) was obtained and special attention has been paid to characterize the transition from coherent to incoherent motion and to determine the diffusion coefficient.

Nevertheless, most of these works were applied to Hamiltonians that conserve the polaron population. However, in proteins, the amide-I energy relaxation is very fast and recent experiments have clearly shown that the polaron lifetime is typically of about $T_1=1.5$ ps [30–37]. The relaxation originates from intramolecular energy redistribution due to the anharmonic coupling between each amide-I mode and a set of intramolecular normal modes whose displacements are strongly localized on the C=O groups [38,39].

In that context, the aim of the present paper is to describe how the amide-I relaxation modifies the polaron transport properties in α helices. To proceed, the original Davydov model is first modified to account for the additional interactions between the amide-I modes and a bath of intramolecular normal modes. Then, because the observed lifetime is very short, non-Markovian effects are expected to affect the polaron dynamics in the short time limit. The GME is thus established by using the so-called time-convolutionless (TCL) approach which is local in time and allows a systematic analysis of the non-Markovian dynamics of open systems. Moreover, to second order in the coupling strength, it gives a better approximation to the exact solution than the standard GME [40–47].

The present work is motivated by recent studies in which it has been pointed out that the amide-I relaxation may play a key role in various biological processes. Indeed, as suggested by Cruzeiro and co-workers [48,49], the energy released by the decay of the amide-I mode can be used by the helix to change its conformation. Similarly, within a one-site Davydov model, it has been shown that this relaxation is responsible for a softening of the H bond and it may be a precursor to the H bond breaking [50]. Finally, it has been suggested that amide-I relaxation may appear as an intermediate agent in electron capture dissociation (ECD) allowing H hopping between two peptide units and giving rise to the cleavage of the nearby N-C_α bond [51]. Nevertheless, in all these previous works, the dipole-dipole coupling has been disregarded so that the fundamental question arises whether

*vincent.pouthier@univ-fcomte.fr

the polaron mobility modifies these processes.

The paper is organized as follows. In Sec. II, the modified Davydov model is first presented and the key observables required to study the transport properties are introduced. Then, the small polaron point of view is summarized. In Sec. III, the GME for the polaron RDM is established and the vibron mean square displacement is evaluated in Sec. IV. The GME is solved numerically in Sec. V where a detailed analysis of the energy transfer is performed. Finally, these results are discussed and interpreted in Sec. VI.

II. DESCRIPTION OF THE SYSTEM

A. Hamiltonians and transport properties

As detailed in numerous papers [7–10], the vibron-phonon dynamics in α helices reduces to that of a single spine of H-bonded peptide units regularly distributed along a 1D lattice. Each site, whose position is labeled by the index $x=1,\ldots,N$, contains an amide-I mode which behaves as a harmonic oscillator with frequency ω_0. Restricting our attention to the one-vibron dynamics, the xth amide-I mode is equivalent to a two-level system whose first excited state is denoted $|x\rangle$. The zero vibron state, defined as the vacuum state $|\oslash\rangle$, describes all the amide-I modes in their ground state. The vibron Hamiltonian is thus written as (with the convention $\hbar=1$)

$$H_v = \sum_x \omega_0 |x\rangle\langle x| + \Phi[|x+1\rangle\langle x| + |x\rangle\langle x+1|], \tag{1}$$

where Φ is the vibron hopping constant.

The vibron interacts with the peptide unit motions that define the phonons. They describe N acoustic modes with frequency $\Omega_q=\Omega_c|\sin(q/2)|$ and with wave vector q, where $\Omega_c=\sqrt{4W/M}$, M and W being the peptide unit mass and the H bond force constant, respectively. The phonon Hamiltonian is expressed in terms of the boson operators $a_q^\dagger$ and a_q as $H_p=\Sigma_q \Omega_q a_q^\dagger a_q$. The vibron-phonon coupling results from the modulation of each amide-I frequency by the peptide unit motions as

$$\Delta H = \sum_x \left[\sum_q (\Delta_{qx} a_q^\dagger + \Delta_{qx}^* a_q) \right] |x\rangle\langle x|, \tag{2}$$

where $\Delta_{qx}=-i\Delta_0 \sin(q)/\sqrt{|\sin(q/2)|}e^{-iqx}/\sqrt{N}$ involves the parameter χ introduced in the original Davydov model as $\Delta_0=\chi(\hbar^2 MW)^{-1/4}$ ($\hbar$ has been reintroduced to avoid confusion).

Following recent works detailed in Refs. [50,51], the energy relaxation is assumed to result from Fermi resonances involving the xth amide-I mode and either overtones or combination bands of a set of intramolecular normal modes. These normal modes, whose displacements are strongly localized on the xth C=O group, belong typically to the 500–1000 cm^{-1} region (see, for instance, Ref. [30]). Note that other relaxation pathways may be involved in the relaxation, such as the direct resonance with a high-frequency mode, but they will be disregarded in the present study.

The intramolecular normal modes are described by harmonic oscillators with frequency ω_α and boson operators $b_{\alpha x}$ and $b_{\alpha x}^\dagger$. They define a thermal bath attached to the xth peptide unit so that the vibron interacts with a set of independent baths whose Hamiltonian is $H_B=\Sigma_{x\alpha}\omega_\alpha b_{\alpha x}^\dagger b_{\alpha x}$. This thermal bath allows for energy exchanges mediated by Fermi resonances involving one vibron and two bath excitations as

$$V = \sum_{\alpha\beta x} \Delta_{\alpha\beta}(x) b_{\alpha x}^\dagger b_{\beta x}^\dagger |\oslash\rangle\langle x| + \Delta_{\alpha\beta}^*(x) b_{\alpha x} b_{\beta x} |x\rangle\langle\oslash|, \tag{3}$$

where $\Delta_{\alpha\beta}(x)$ is the coupling strength between the xth amide-I mode and the modes α and β of the xth bath. Note that since the density of normal modes in the 500–1000 cm^{-1} region is rather large [39,52–54], the relevant modes of the bath cannot be significantly thermally excited. The bath is unable to supply energy to the amide-I modes and it is just responsible for vibron annihilation.

The spine dynamics is thus governed by the full Hamiltonian $H=H_v+H_p+H_B+\Delta H+V$ which does not conserve the vibron number. Without any perturbation, the spine is in thermal equilibrium at temperature T. Since $\omega_0\approx 1660\ \mathrm{cm}^{-1}$, each amide-I mode lies in its ground state whereas both the phonons and the thermal bath are described by standard Boltzmann distributions ρ_p and ρ_B, respectively. Therefore, to study the vibrational energy flow we assume that the spine reaches a configuration out of equilibrium in which one vibron is created on the site $x_0=0$. The initial density matrix is thus $\rho=\rho_v\otimes\rho_B\otimes\rho_p$, where $\rho_v=|x_0\rangle\langle x_0|$ denotes the vibron density matrix. Note that such an excitation may result from the energy released by the hydrolysis of ATP [1] or from charge neutralization upon electron capture by a protonated α helix [51].

To characterize the vibrational energy flow, let the vibron density $P(x,t)$ define the average vibron number on the xth site at time t as

$$P(x,t) = \mathrm{Tr}[\rho e^{iHt}|x\rangle\langle x|e^{-iHt}]. \tag{4}$$

It is the central object of the present study whose knowledge allows one to compute, in principle, all the required observables to describe the energy redistribution. Among the different observables, we shall focus our attention on the vibron mean square displacement (VMSD) $\langle x^2(t)\rangle$ whose time evolution gives fundamental information. Indeed, according to standard transport theories, $\langle x^2(t)\rangle$ scales as t^2 in the short time limit indicating a coherent energy transfer. By contrast, both dephasing-limited coherent motion and phonon-induced incoherent hops lead to diffusion so that $\langle x^2(t)\rangle\approx 2Dt$ in the long time limit, D being the diffusion coefficient. Finally, due to vibron lifetime, we expect a singular behavior of $\langle x^2(t)\rangle$ indicating that energy relaxation-induced localization.

B. Small polaron and reduced density matrix

In α helices at biological temperature, the vibron-phonon coupling predominates over the dipole-dipole interaction and the strong-coupling nonadiabatic limit is reached. The dynamics is dominated by the so-called dressing mechanism and it is more efficient to work with a dressed vibron basis rather than with a delocalized bare vibron basis [5–10]. Note that although such an approach is clearly justified at biological temperature, it becomes questionable at very low temperature, i.e., typically in the range 13–53 K, where a tran-

sition takes place between the strong- and weak-coupling limit (see, for instance, Refs. [2–6,19,55]).

To reach the dressed point of view, a two-step procedure is used. First, to partially remove ΔH, a Lang-Firsov transformation is applied [15]. Then, a mean-field procedure is used so that the transformed Hamiltonian is expressed as the sum of five separated contributions as $\hat{H}=H_{\rm po}+H_p+H_B+\Delta\hat{H}+\hat{V}$. The polaron Hamiltonian is written as

$$H_{\rm po}=\sum_x(\omega_0-E_B)|x\rangle\langle x|+\hat{\Phi}[|x+1\rangle\langle x|+|x\rangle\langle x+1|], \quad (5)$$

where $E_B=2\Delta_0^2/\Omega_c$ is the small polaron binding energy and $\hat{\Phi}=\Phi{\rm Tr}_p(\rho_p\Theta_x^\dagger\Theta_{x\pm1})$ is the effective hopping constant defined in terms of the dressing operator

$$\Theta_x=\exp\left[-\sum_q\left(\frac{\Delta_{qx}}{\Omega_q}a_p^\dagger-\frac{\Delta_{qx}^*}{\Omega_q}a_p\right)\right]. \quad (6)$$

In this new point of view, $|x\rangle$ defines a small polaron on the xth site that corresponds to a vibron dressed by a lattice distortion specified by the state $\Theta_x|x\rangle$ in the original point of view. The dressing prevents the delocalization of the polaron whose effective hopping constant $\hat{\Phi}$ is smaller than the bare constant Φ and it yields a redshift of the vibrational frequency of each amide-I mode.

In that context, the remaining polaron-phonon coupling originates from the modulation of the hopping terms by the dressing operator fluctuations as

$$\Delta\hat{H}=\sum_x\Delta\Phi_{x+1,x}|x+1\rangle\langle x|+{\rm H.c.}, \quad (7)$$

where H.c. stands for Hermitian conjugate and where $\Delta\Phi_{x,x'}=(\Phi\Theta_x^\dagger\Theta_{x'}-\hat{\Phi})\delta_{|x-x'|,1}$. Similarly, the polaron-thermal bath interaction results from Fermi resonances which are now accompanied by phonon exchanges as

$$\hat{V}=\sum_{\alpha\beta x}\Delta_{\alpha\beta}(x)b_{\alpha x}^\dagger b_{\beta x}^\dagger\Theta_x|\oslash\rangle\langle x|+{\rm H.c.} \quad (8)$$

In the polaron point of view, the invariance of $|x\rangle\langle x|$ under the Lang-Firsov transformation makes the study of the transport properties easier. Indeed, the vibron density is equivalent to the polaron density so that Eq. (4) is simply rewritten as

$$P(x,t)={\rm Tr}[\hat{\rho}e^{i\hat{H}t}|x\rangle\langle x|e^{-i\hat{H}t}]. \quad (9)$$

The time evolution is now governed by $\hat{H}$ and the initial statistical average is performed with respect to the transformed density matrix $\hat{\rho}=\rho\rho_c$. Since the vibron creation yields a polaron accompanied by a lattice distortion, ρ_c measures the initial correlations between the polaron and the phonons. Nevertheless, it is straightforward to show that ρ_c is proportional to $\exp(-E_B/kT)$ at biological temperature (k being the Boltzmann constant). Since E_B typically extends from 4 to 16 $\rm cm^{-1}$ [7], the initial correlations can be neglected and the approximation $\rho_c\approx1$ will be used.

Finally, a complete characterization of the vibron density required to introduce a more general object, namely, the so-called polaron RDM $\sigma(t)$ defined as

$$\sigma(x_1,x_2,t)={\rm Tr}[\rho e^{i\hat{H}t}|x_2\rangle\langle x_1|e^{-i\hat{H}t}]. \quad (10)$$

The RDM describes the polaron state at time t after performing an average over both the phonons and the thermal bath. Diagonal elements yield the vibron density, i.e., $P(x,t)=\sigma(x,x,t)$, whereas nondiagonal elements measure the coherence between dressed states. Under the influence of $\hat{H}$, diagonal and nondiagonal elements interact so that the time evolution of the full RDM must be studied to extract the information that is desired. The following section is thus devoted to the derivation of a GME to characterize the RDM evolution.

III. TIME-CONVOLUTIONLESS GME

A. General expression of the GME

To determine the GME for the polaron RDM, the standard projector method of the TCL approach is used [40–47]. To proceed, let $\mathcal{B}$ define the superbath that includes both the phonons and the bath of intramolecular normal modes. It is described by the density matrix $\rho_{\mathcal{B}}=\rho_B\otimes\rho_p$ so that we can split the trace in Eq. (10) into partial traces to rewrite the RDM as

$$\sigma(x_1,x_2,t)={\rm Tr}_{\rm po}[\rho_v Pe^{i\mathcal{L}t}P|x_2\rangle\langle x_1|]. \quad (11)$$

The projector $P\cdots={\rm Tr}_{\mathcal{B}}[\rho_{\mathcal{B}}\cdots]$ realizes an average over the superbath simply noted $\langle\cdots\rangle$ and $\mathcal{L}=[\hat{H},\ldots]$ is the system Liouvillian. In that context, by performing a second order expansion with respect to both $\Delta\hat{H}$ and $\hat{V}$, the GME for the polaron RDM is expressed as

$$i\dot{\sigma}(x_1,x_2,t)=\hat{\Phi}\sum_{s=\pm1}[\sigma(x_1+s,x_2,t)-\sigma(x_1,x_2+s,t)]-i\sum_{\bar{x}_1,\bar{x}_2}\mathcal{J}(x_1,x_2,\bar{x}_1,\bar{x}_2,t)\sigma(\bar{x}_1,\bar{x}_2,t). \quad (12)$$

The first term on the right-hand side of Eq. (12) describes the coherent dynamics under the influence of the polaron Liouvillian $\mathcal{L}_{\rm po}=[H_{\rm po},\ldots]$. By contrast, the influence of the coupling with the superbath is characterized by the time-dependent relaxation operator $\mathcal{J}(t)$ whose matrix elements are defined as

$$\mathcal{J}(x_1,x_2,\bar{x}_1,\bar{x}_2,t)=[\Gamma_{x_1,\bar{x}_1}(t)+\gamma_{x_1,\bar{x}_1}(t)]\delta_{x_2,\bar{x}_2}+[\Gamma_{x_2,\bar{x}_2}^*(t)+\gamma_{x_2,\bar{x}_2}^*(t)]\delta_{x_1,\bar{x}_1}-[W_{x_1,\bar{x}_1,x_2,\bar{x}_2}(t)+W_{x_2,\bar{x}_2,x_1,\bar{x}_1}^*(t)]. \quad (13)$$

The different contributions of $\mathcal{J}(t)$ involve correlation functions of the polaron-superbath interactions. They correspond to an average over the superbath of operators whose time dependence refers to a Heisenberg representation with respect to the unperturbed Hamiltonian $H_0=H_{\rm po}+H_p+H_B$.

In that context, the coupling between the polaron and the bath of intramolecular normal modes gives rise to the contribution $\gamma(t)$ expressed as

$$\gamma_{x_1,\bar{x}_1}(t) = \int_0^t d\tau f_B(x_1,\tau) C_{x_1}(\tau) G^*_{x_1,\bar{x}_1}(\tau), \tag{14}$$

where $G(t)=\exp(-H_{\rm po}t)$ is the polaron free propagator $C_x(t)=\langle \Theta_x^\dagger(t)\Theta_x(0)\rangle$ is the dressing operator correlation function and $f_B(x,t)$ is the thermal bath correlation function written as

$$f_B(x,t) = \sum_{\alpha\beta} \Delta^2_{\alpha\beta}(x)\langle b_{\alpha x}(t) b_{\beta x}(t) b^\dagger_{\alpha x} b^\dagger_{\beta x}\rangle. \tag{15}$$

In Eq. (13), both $\Gamma(t)$ and $W(t)$ refer to the polaron-phonon interaction as

$$\Gamma_{x_1,\bar{x}_1}(t) = \sum_x \sum_{s=\pm 1} \int_0^t d\tau [C_+^{x_1,s}(x,\tau) G_{0,x}(\tau) G^*_{0,x_1-\bar{x}_1+x}(\tau) + C_-^{x_1,s}(x,\tau) G_{0,x-s}(\tau) G^*_{0,x_1-\bar{x}_1+x+s}(\tau)],$$

$$W_{x_1,\bar{x}_1,x_2,\bar{x}_2}(t) = \sum_x \sum_{s=\pm 1} \delta_{x_2,\bar{x}_2+s} \int_0^t d\tau \times [C_+^{\bar{x}_2,s}(x,\tau) G_{0,x_2-x_1+x}(\tau) G^*_{0,\bar{x}_2-\bar{x}_1+x}(\tau) + C_-^{\bar{x}_2,s}(x,\tau) G_{0,x_2-x_1+x-s}(\tau) G^*_{0,\bar{x}_2-\bar{x}_1+x+s}(\tau)], \tag{16}$$

where the correlation functions $C_\pm^{y,s}(x,t)$ are defined as

$$C_+^{y,s}(x,t) = \langle \Delta\Phi_{y,y+s}(t) \Delta\Phi_{y+s+x,y+x}(0)\rangle,$$

$$C_-^{y,s}(x,t) = \langle \Delta\Phi_{y,y+s}(t) \Delta\Phi_{y+x,y+s+x}(0)\rangle. \tag{17}$$

According to Eq. (12), the polaron-superbath interaction leads to a coupling between two coherences $\sigma(x_1,x_2,t)$ and $\sigma(\bar{x}_1,\bar{x}_2,t)$. Although this coupling is local in time, it results from the history of the interaction. Basically, a coupling occurs if an interaction involving the states $|x_1\rangle$ or $|x_2\rangle$ at time t is induced by the superbath which keeps the memory of a past interaction involving states at time $t-\tau$ whose free evolution yields $|\bar{x}_1\rangle$ or $|\bar{x}_2\rangle$ at time t.

The GME is isomorphic to the Schrödinger equation for a single particle moving on a two-dimensional (2D) lattice. This lattice is a graphical representation of the Liouville space in which the site position is defined by the two indexes (x_1,x_2). The RDM plays the role of a wave function whose dynamics is governed by the time dependent effective Liouvillian $\mathcal{L}_{\rm po}-i\mathcal{J}(t)$. Within this equivalence, $\mathcal{L}_{\rm po}$ gives rise to an anisotropic dynamics which is translationally invariant along the directions x_1 and x_2. However, a symmetry breaking is induced by $\mathcal{J}(t)$ which prevents this 2D translational invariance. Nevertheless, as illustrated in the Appendix, the parameters that define $\mathcal{J}(t)$ exhibit specific properties. Indeed, both the thermal bath and the dressing operator correlation functions do not depend on the site position. They will be denoted $f_B(t)$ and $C(t)$, respectively. Similarly, $C_\pm^{y,s}(x,t) \equiv C_\pm(x,t)$ only depend on the distance $|x|$. Therefore $\mathcal{J}(x_1,x_2,\bar{x}_1,\bar{x}_2,t)$ is a function of x_1-x_2, $\bar{x}_1-\bar{x}_2$, $\bar{x}_2-x_2$, and $\bar{x}_1-x_1$, only, so that the 2D Liouville space remains translationally invariant along the direction $x_1=x_2$.

Consequently, the RDM $\sigma(x_1,x_2,t)$ only depends on x_1 and $m=x_2-x_1$, and it can be expanded as a Bloch wave as [56]

$$\sigma(x_1,x_1+m,t) = \frac{1}{Ni^m} \sum_k \Psi_k(m,t) e^{-ik(x_1+m/2)}. \tag{18}$$

The momentum k, which takes N values belonging to the first Brillouin zone of the spine, describes the RDM delocalization along the direction $x_1=x_2$. Since k is a good quantum number, the effective Liouvillian is block diagonal and the GME can be solved for each k value as

$$i\dot{\Psi}_k(m,t) = \tilde{\Phi}_k[\Psi_k(m+1,t) + \Psi_k(m-1,t)] - i\sum_{\bar{m}} \mathcal{J}_k(m,\bar{m},t)\Psi_k(\bar{m},t), \tag{19}$$

where $\tilde{\Phi}_k=2\hat{\Phi}\sin(k/2)$ and where the matrix elements of $\mathcal{J}_k(t)$ are defined as

$$\mathcal{J}_k(m,\bar{m},t) = 2i^{m-\bar{m}} \,\mathrm{Re} \int_0^t e^{-ik(m-\bar{m})/2} d\tau \times \Bigg[f_B(\tau) C(\tau) G^*_{0,m-\bar{m}}(\tau) + \sum_{x,s} C_+(x,\tau) G_{0,x}(\tau) G^*_{0,m-\bar{m}+x}(\tau) + \sum_{x,s} C_-(x,\tau) G_{0,x-s}(\tau) G^*_{0,m-\bar{m}+x+s}(\tau) - \sum_{x,s} C_+(x,\tau) G_{0,m+x}(\tau) G^*_{0,\bar{m}+x}(\tau) e^{iks} - \sum_{x,s} C_-(x,\tau) G_{0,m+x-s}(\tau) G^*_{0,\bar{m}+x+s}(\tau) e^{iks} \Bigg]. \tag{20}$$

The resulting master equation (19) is isomorphic to the Schrödinger equation for a single particle moving on a 1D lattice whose site position is specified by the index m. Nevertheless, Eq. (20) shows that the relaxation operator still exhibits a very complex nature due to its dependence on the various correlation functions. Therefore, to make to resolution of the GME easier, relevant approximations must be invoked as shown in the next section.

B. Approximated expression of the GME

To simplify the GME, let first consider the first term in the right-hand side of Eq. (20). This term, which describes polaron energy relaxation, measures the system memory at time t of a transition induced by the polaron-thermal bath coupling at $t=0$. It involves three contributions. First, the vibron creation modifies the phonon state and it yields a lattice distortion in the vicinity of the excited site. This distortion propagates along the lattice with sound velocity and its memory is accounted by $C(t)$. Then, due to Fermi resonances the thermal bath reaches a coherent superimposition of number states. As time evolves, each contribution of that superimposition varies according to its own frequency so that the

coherence tends to disappear. The memory of this initial excitation is thus described by $f_B(t)$. Finally, the polaron propagates along the lattice and the memory of its initial position is given by the free propagator $G^*_{0,m-\bar{m}}(t)$. As shown in Ref. [51], $f_B(t)C(t)$ decays in split picoseconds at biological temperature. This time scale is very short when compared with the time $\hat{\Phi}^{-1}$ required to a polaron to cover a lattice site. Consequently, the polaron does not have enough time to move and the Markov limit is rapidly reached. Only diagonal terms $m=\bar{m}$ contribute significantly to energy relaxation which is characterized by the time-dependent decay rate

$$\gamma_0(t) = 2\,\mathrm{Re}\int_0^t d\tau f_B(\tau)C(\tau)G^*_{0,0}(\tau). \tag{21}$$

Similarly, the terms involving $C_\pm(x,t)$ in Eq. (20) measure the system memory at time t of a polaron-phonon interaction occurring at $t=0$. As detailed in Ref. [47], an initial interaction favors a polaron hop between two neighboring sites. This hop is responsible for a contraction of the H bond that links the two sites. The memory of this process is characterized by two contributions. First, the free propagation of the polaron from the two sites involved in the interaction is characterized by the product between an advanced and a retarded polaron free propagator. Then, the time evolution of the lattice contraction which propagates along the spine is described by $C_\pm(x,t)$ which measures the lattice memory at time t and on site x of a deformation produced at $t=0$ and on the site $x=0$. From the Appendix, we have verified that $C_\pm(x,t)$ describes the propagation of an acoustic wave packet. For a fixed x value, it behaves as a bell-shaped peak centered on the propagating time $\tau_p \approx 2|x|/\Omega_c$ and whose width is about the phonon correlation time $\tau_c = 2/\Omega_c$. Since in α helices $\Omega_c \gg \hat{\Phi}$, the phonons propagate faster than the polaron and the phonon correlations occur over a time scale which is very short when compared with the time required for a polaron to move. Consequently, the main contributions of the relaxation operator involve terms in which an advanced polaron propagator exactly compensates the associated retarded propagator. The polaron-phonon interaction is thus characterized by the two relaxation rates

$$\Gamma^\pm_m(t) = 2\,\mathrm{Re}\sum_x \int_0^t d\tau C_\pm(x,\tau)|G_{0,m+x}(\tau)|^2. \tag{22}$$

By using the previously discussed approximations, the time-dependent relaxation operator is finally rewritten as

$$\begin{aligned}\mathcal{J}_k(m,\bar{m},t) = {} & \delta_{\bar{m},m}[\gamma_0(t) + 2\Gamma^+_0(t) - 2\cos(k)\Gamma^+_m(t)] \\ & + \delta_{\bar{m},m+2}[\Gamma^-_{m+1}(t) - \cos(k)\Gamma^-_1(t)] \\ & + \delta_{\bar{m},m-2}[\Gamma^-_{m-1}(t) - \cos(k)\Gamma^-_1(t)].\end{aligned} \tag{23}$$

Each term in Eq. (23) describes a well-defined relaxation pathway in the 2D Liouville space. Indeed, the energy relaxation characterized by $\gamma_0(t)$ yields a decay of each polaron RDM matrix element. By contrast, $\Gamma^+_m(t)$ leads to oblique transitions $(x_1,x_2)\to(x_1\pm 1,x_2\pm 1)$. For $x_2=x_1$ $(m=0)$, it couples two populations and it defines the time-dependent transition rate for incoherent polaron hops mediated by lattice phonons. This term also contributes to dephasing and it gives rise to a decay of the nondiagonal RDM elements. Similarly, $\Gamma^-_m(t)$ refers to phonon-induced coherence transfers between nondiagonal RDM elements. It first accounts for both horizontal $(x_1,x_2)\to(x_1\pm 2,x_2)$ and vertical $(x_1,x_2)\to(x_1,x_2\pm 2)$ transitions and it also contributes to antioblique transitions $(x_1,x_2)\to(x_1\pm 1,x_2\mp 1)$.

Finally, by inserting Eq. (23) into Eq. (19) we obtain a simplified version of the GME which is isomorphic to a 1D Schrödinger equation for $\Psi_k(m,t)$ with nearest- and next-nearest-neighbor time-dependent couplings. This equation can be solved numerically for each k value to determine the time evolution of the vibron density as illustrated in Sec. V. Nevertheless, before presenting these results, an approximate expression of the VMSD is established in the next section which allows us to introduce key parameters to characterize the energy transport.

IV. MEAN SQUARE DISPLACEMENT

From Eq. (18), the VMSD is defined as

$$\langle x^2(t)\rangle = -\left(\frac{\partial^2\Psi_k(0,t)}{\partial k^2}\right)_{k=0}. \tag{24}$$

Its time evolution is governed by the long-wavelength behavior of the restriction $\Psi_k(0,t)$ to the site $m=0$. This behavior can be extracted from the GME by applying a standard perturbation theory in which k is assumed to be a small parameter. To proceed, we define $\Psi_k(m,t)$ as the component of the vector $|\Psi(t)\rangle$ in the site representation $\{|m\rangle\}$. At time $t=0$, the polaron creation on the site $x_0=0$ gives rise to the initial condition $|\Psi(0)\rangle=|0\rangle$. By expanding Eq. (19) to second order with respect to k, the time evolution of $|\Psi(t)\rangle$ is governed by the Schrödinger-like equation

$$i|\dot{\Psi}(t)\rangle = [\mathcal{H}_0(t) + \mathcal{V}_1(t)k + \mathcal{V}_2(t)k^2 + \cdots]|\Psi(t)\rangle, \tag{25}$$

where $\mathcal{H}_0(t) = -i\mathcal{J}_{k=0}(t)$ and where

$$\begin{aligned}\mathcal{V}_1(m,\bar{m},t) &= \hat{\Phi}[\delta_{\bar{m},m+1} + \delta_{\bar{m},m-1}], \\ \mathcal{V}_2(m,\bar{m},t) &= -i\Gamma^+_m(t)\delta_{\bar{m},m} - i\frac{\Gamma^-_1(t)}{2}[\delta_{\bar{m},m+2} + \delta_{\bar{m},m-2}].\end{aligned} \tag{26}$$

The general solution of Eq. (25) is given by the so-called evolution operator $U(t)$ satisfying $|\Psi(t)\rangle = U(t)|\Psi(0)\rangle$ and which is expanded as

$$U(t) = U^{(0)}(t) + U^{(1)}(t)k + U^{(2)}(t)k^2 + \cdots. \tag{27}$$

In that context, the VMSD is proportional to the restriction $U^{(2)}_{00}(t)$ to the subspace generated by $|0\rangle$ and it depends on the evolution operator $U^{(0)}(t)$ connected to $\mathcal{H}_0(t)$. From Eq. (23), $\mathcal{H}_0(t)$ exhibits two contributions. First, its diagonal part $\mathcal{H}_0(m,m,t) = -i\lambda_m(t)$ provides to each site m a damping constant $\lambda_m(t) = \gamma_0(t) + 2[\Gamma^+_0(t) - \Gamma^+_m(t)]$. Then, its nondiagonal part gives rise to couplings between next-nearest-neighbor

sites as $\mathcal{H}_0(m,m\pm 2,t)=-i[\Gamma^-_{m\pm 1}(t)-\Gamma^-_1(t)]$. Consequently, $\mathcal{H}_0(t)$ is block diagonal, the site $m=0$ being independent from the other sites, and $U^{(0)}_{00}(t)$ is written as

$$U^{(0)}_{00}(t)=\exp\left[-\int_0^t dt_1\gamma_0(t_1)\right]. \tag{28}$$

Since $\gamma_0(t)$ rapidly converges, it can be approximated by a constant value $\gamma_0=\gamma_0(t\to\infty)$. After simple algebraic manipulations, the VMSD is thus expressed as

$$\langle x^2(t)\rangle = 2e^{-\gamma_0 t}\int_0^t dt_1\Gamma^+_0(t_1) + 2e^{-\gamma_0 t}\hat{\Phi}^2\int_0^t dt_1\int_0^{t_1} dt_2 e^{\gamma_0(t_1-t_2)}\mathcal{G}(t_1,t_2), \tag{29}$$

where $\mathcal{G}(t_1,t_2)$ is defined as

$$\mathcal{G}(t_1,t_2)=\sum_{m=\pm 1}\sum_{m'=\pm 1}\langle m|U^{(0)}(t_1)U^{(0)}(t_2)^{-1}|m'\rangle. \tag{30}$$

As will be shown in the next section, the time evolution of $\Gamma^\pm_m(t)$ reveals two main features. First, for small m values, $\Gamma^\pm_m(t)$ rapidly converges to a constant value $\Gamma^\pm_m=\Gamma^\pm_m(t\to\infty)$. Then, the sites $m=\pm 1$ are preferentially coupled one to each other under the influence of $\mathcal{H}_0(t)$ because $\Gamma^\pm_m-\Gamma^\pm_1$ takes significant value for $m=0$, only. Consequently, in the subspace $m=\pm 1$, $\mathcal{H}_0(t)$ is well described by a (2×2) matrix whose diagonal and nondiagonal elements reduce to $-i\lambda_1$ and $-i(\Gamma^-_0-\Gamma^-_1)$, respectively. This representation makes the evaluation of $\mathcal{G}(t_1,t_2)$ easier so that the VMSD is finally expressed as

$$\langle x^2(t)\rangle = e^{-\gamma_0 t}\left(2\Gamma^+_0 t+\frac{4\hat{\Phi}^2}{\Gamma^*}\left[t+\frac{e^{-\Gamma^* t}-1}{\Gamma^*}\right]\right), \tag{31}$$

where $\Gamma^*=2[\Gamma^+_0-\Gamma^+_1]+[\Gamma^-_0-\Gamma^-_1]$

As shown in Eq. (31), the VMSD slightly differs form the usual expression which arises from the standard transport theory. It exhibits two contributions. The first contribution corresponds to the exponential decay $\exp[-\gamma_0 t]$ which describes the irreversible polaron relaxation over the bath of intramolecular normal modes. This decay occurs over a time scale given by the polaron lifetime defined as $T_1=1/\gamma_0$. The second contribution, defined by the term in brackets in the right-hand side of Eq. (31), is the standard VMSD which arises when the vibron number is conserved. It describes the motion of the polaron due to both its ability to delocalize along the lattice and its coupling with the lattice phonons.

The influence of the polaron-phonon interaction is twofold. First, it is responsible for random fluctuations of the polaron hopping constants which give rise to incoherent transitions between nearest-neighbor sites. The corresponding rate defines the so-called incoherent diffusion coefficient $D_i=\Gamma^+_0$. Then, the phonons yield dephasing characterized by the rate Γ^*. Formally, if a polaron moves in a coherent manner, its eigenstate is a superimposition of localized states whose phases are related to each other when the evolution is governed by $H_{\rm po}$, only. However, the coupling with the bath induces fluctuations of each phase which destroy the coherence. The nature of the motion evolves from a coherent to an incoherent one over a time scale given by the dephasing time $T_2=1/\Gamma^*$. The incoherent regime is characterized by the coherent diffusion coefficient $D_c=2\hat{\Phi}^2/\Gamma^*$.

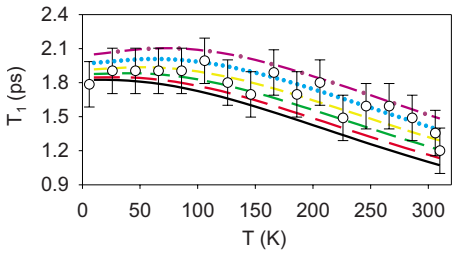

FIG. 1. (Color online) T_1 vs T for $\chi=30$ pN (full line), $\chi=36$ pN (long dashed line), $\chi=42$ pN (medium dashed line), $\chi=48$ pN (short dashed line), $\chi=54$ pN (dotted line), and $\chi=60$ pN (dashed dotted line). Open circles represent experimental data extracted from Ref. [30].

V. NUMERICAL RESULTS

In this section, the previous formalism is applied to study the polaron motion in a 1D lattice of H-bonded peptide units. To proceed, typical values for the parameters are used: $\omega_0=1660$ cm^{-1}, $\Phi=7.8$ cm^{-1}, $W=11$ N m^{-1}, and $M=2.0\times 10^{-25}$ kg. The typical range $\chi=30-60$ pN is considered for the vibron-phonon coupling strength.

To describe the interaction with the bath, the coupling distribution in the frequency domain is modeled by a Gaussian law centered around $\omega_c=\omega_0/2$ [50,51]. In the time domain, the thermal bath correlation function is thus written as

$$f_B(t)=\frac{G(T)}{\pi}\exp[-\alpha^2 t^2-2i\omega_c t], \tag{32}$$

where $\alpha=50$ cm^{-1} is the Fermi resonance bandwidth. In practice, $G(T)$ is a function of the temperature through its dependence on the populations of the intramolecular normal modes. To mimic this feature, we use the following phenomenological law: $G(T)=G_0[1+(T/T_0)^2]$, where $G_0=265$ cm^{-2} and $T_0=310$ K.

The temperature dependence of the polaron lifetime is displayed in Fig. 1. Open circles refer to experimental data describing the amide-I lifetime in myoglobin [30]. At high temperature, T_1 decreases almost linearly with T whatever the strength χ of the vibron-phonon coupling. However, at low temperature, T_1 slightly decreases with T for small χ values, only. Indeed, for strong couplings, T_1 first increases to reach a maximum value around $T=50$ K and then develops a linear decay. Nevertheless, in the range $\chi=30-60$ pN, our numerical results are in a relatively good agreement with the experimental data. They reveal that T_1 typically ranges between 1.5 and 2 ps. The polaron lifetime weakly depends on the temperature and it slightly increases with χ.

The polaron-phonon interaction is accounted by the rates $\Gamma^\pm_m(t)$ [Eq. (22)] whose time evolution has been studied numerically for $T=310$ K and $\chi=45$ pN. Two situations occur depending on whether $m=0$ or not. Indeed, after a time scale

of about the phonon correlation time $\tau_c=0.14$ ps, $\Gamma_0^+(t)$ rapidly converges to a constant value $\Gamma_0^+=2.1$ cm^{-1}. By contrast, for $m\neq 0$, $\Gamma_m^+(t)$ turns on after a time scale of about the phonon propagation time $\tau_p\approx m\tau_c$. Then, it converges to a constant value almost m independent and typically about 1.0 cm^{-1}. Similarly, $\Gamma_0^-(t)$ rapidly reaches its Markov limit $\Gamma_0^-=-0.23$ cm^{-1} but by exhibiting small oscillations in the very short time limit. For $m\neq 0$, the signature of the phonon propagation still occurs so that $\Gamma_m^-(t)$ turns on after a time $\tau_p\approx m\tau_c$. Its Markov limit, about $\Gamma_m^-\approx -0.34$ cm^{-1}, is still almost m independent. Note that such a behavior legitimizes the approximations used in Sec. IV to evaluate the VMSD.

To characterize the vibrational energy redistribution, the time evolution of the vibron density $P(x,t)$ is shown in Fig. 2 for $x=0,\ldots,5$ and for $T=310$ K. For small χ values ($\chi=30$ pN), Fig. 2(a) reveals that the population of the excited site $P(0,t)$ exhibits different regimes (see the inset). Over one ps, it first rapidly decreases according to a Gaussian law modulated by an exponential decay. Then, it evolves rather slowly around $P(0,t)\approx 0.025$ until time reaches 2 ps. Finally, for $t>2$ ps, $P(0,t)$ shows an exponential decay according to the damping time $\tau=1.02$ ps. As displayed in Figs. 2(b)–2(f) (full line), this energy decay gives rise to the propagation of the polaron along the lattice. Therefore, $P(x,t)$ evolves in time according to a bell-shaped peak whose width slightly increases with the position x. However, the figures reveal that $P(x,t)$ experiences a strong damping as the energy propagates along the lattice. For instance, the maximum of the density is equal to 0.13 for $x=1$ whereas it reduces to 4×10^{-3} for $x=5$, indicating that the polaron tends to localize around the excited site.

For larger χ values ($\chi=45$ and 60 pN), Fig. 2(a) shows that $P(0,t)$ decreases in the short time limit. However, it does not reach an intermediate slowly varying regime but it rapidly develops an exponential decay. The corresponding damping time increases with the coupling from $\tau=1.18$ ps for $\chi=45$ pN to $\tau=1.40$ ps for $\chi=60$ pN. In other words, the stronger is the vibron-phonon coupling, the longer is the time required for the energy to leave the excited site. As illustrated in Figs. 2(b)–2(f), a slower energy delocalization occurs. The density evolves in time according to a rather asymmetric peak whose maximum value decreases with χ. However, the asymmetry is enhanced by the coupling so that the stronger is the coupling, the longer is the time spent by the energy on a given site. Finally, a localization enhancement takes place and, for instance, the maximum of the density for $\chi=60$ pN varies from 0.09 for $x=1$ to 3×10^{-4} for $x=5$.

To characterize the localization, let $P_0(x)$ denote the maximum value of $P(x,t)$ occurring at time $t_0(x)$. Its x dependence is illustrated in Fig. 3 for $T=310$ K (full lines). Because the vibron is created on the site $x=0$, $P_0(0)$ is always equal to unity. However, when $x>0$, $P_0(x)$ exhibits an exponential decay. This behavior is rapidly reached for large χ values, i.e., once $x=1$ or 2 [Figs. 3(b) and 3(c)]. By contrast, for $\chi=30$ pN [Fig. 3(a)], the exponential decay occurs for larger x values typically of about $x=5$. The corresponding localization length ξ [i.e., $P_0(x)\propto\exp(-x/\xi)$] decreases with χ and it extends from 0.77 for $\chi=60$ pN to 1.44 for $\chi=30$ pN.

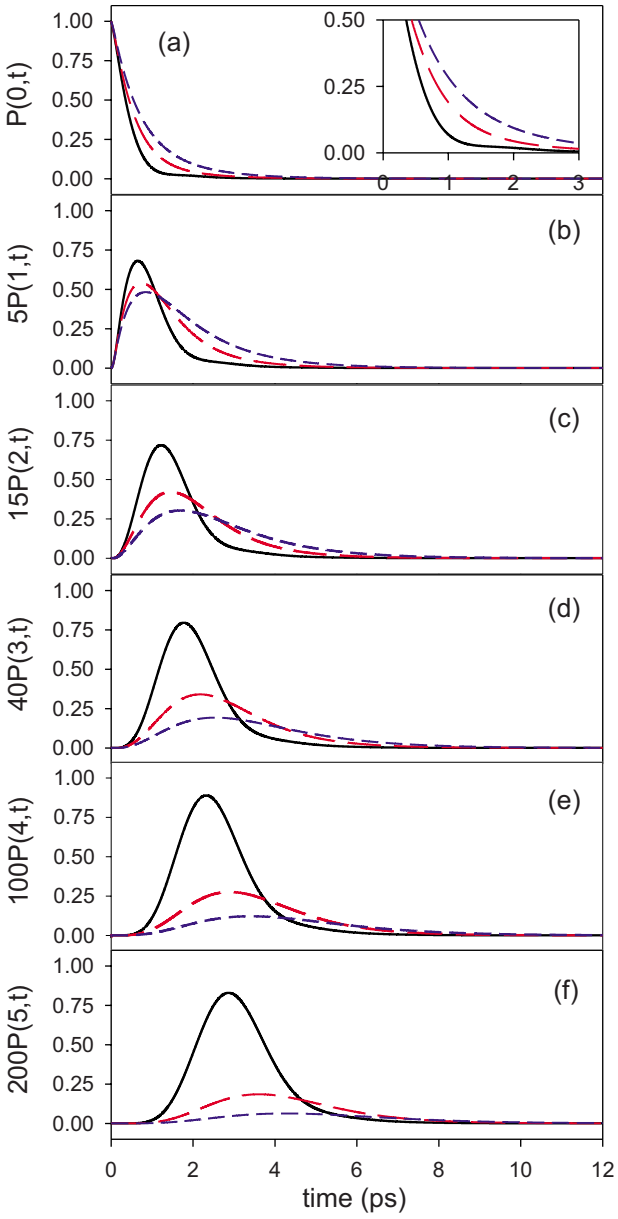

FIG. 2. (Color online) Time evolution of $P(x,t)$ for $T=310$ K for $\chi=30$ pN (full line), $\chi=45$ pN (long dashed line), and $\chi=60$ pN (short dashed line).

Although the localization yields a damping of the density amplitude, Fig. 4 reveals that the energy spreads out with a well-defined velocity. Indeed, $t_0(x)$ increases almost linearly with x which allows us to define the vibrational energy flow velocity as $v_p=[\partial t_0(x)/\partial x]^{-1}$. This velocity clearly decreases with χ and it ranges between 6.27 cm^{-1} (i.e., 1.18 lattice parameter per ps) for $\chi=60$ pN and 9.7 cm^{-1} (i.e., 1.83 lattice parameter per ps) for $\chi=30$ pN. When compared with the polaron group velocity $v_g=2\hat{\Phi}$, it is interesting to note that $v_p\approx 1.10v_g$ for $\chi=30$ pN whereas v_p is about $1.26v_g$ and $4.01v_g$ for $\chi=45$ and 60 pN, respectively.

The VMSD time evolution is illustrated in Fig. 5 for $T=310$ K. Full lines refer to numerical calculations obtained from the GME whereas dashed lines correspond to Eq. (31). In the short time limit, the VMSD scales as t^2 which indi-

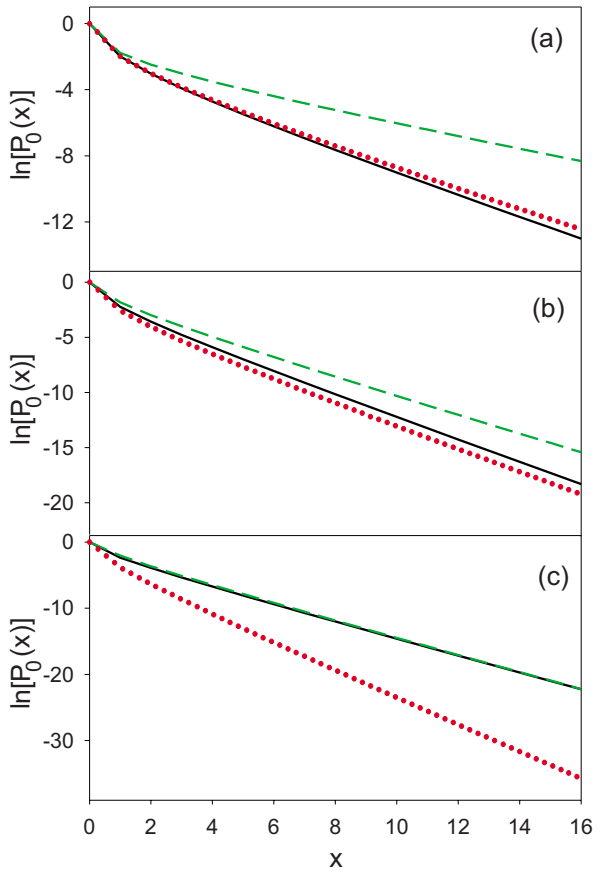

FIG. 3. (Color online) (full lines) $\ln[P_0(x)]$ vs x for (a) $\chi=30$ pN, (b) $\chi=45$ pN, and (c) $\chi=60$ pN and for $T=310$ K. Dotted and dashed lines represent results given by the coherent model and the diffusive model, respectively (see Sec. VI).

cates that the polaron moves coherently along the lattice, as expected from the standard transport theory. Note that a small discrepancy occurs with Eq. (31) which has been obtained by invoking the Markov limit. Then, as time evolves, the VMSD increases to reach a maximum whose value increases when χ decreases. This feature is the signature of the localized behavior of the energy flow which indicates that the polaron explores a finite region of the lattice before its annihilation. Note that at biological temperature, the size of

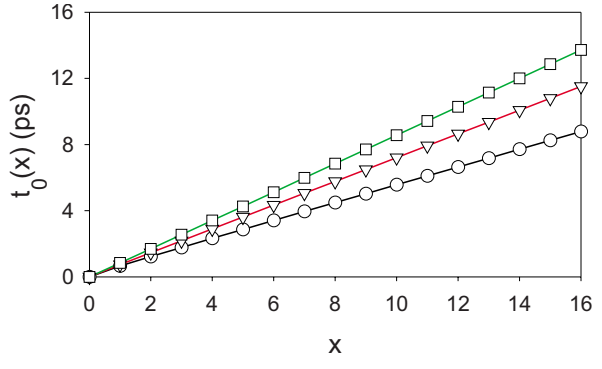

FIG. 4. (Color online) $t_0(x)$ vs x for $T=310$ K and for $\chi=30$ pN (open circles), $\chi=45$ pN (open triangles), and $\chi=60$ pN (open squares).

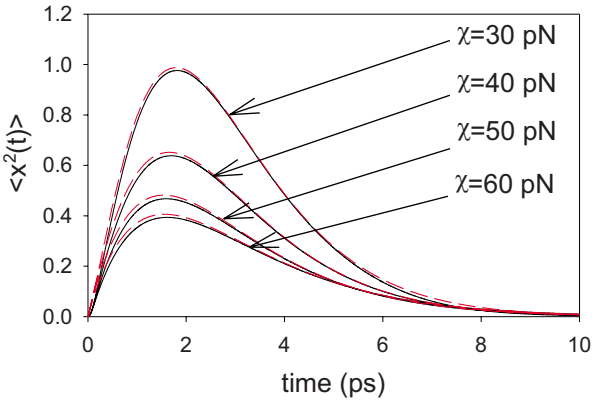

FIG. 5. (Color online) VMSD vs time for $T=310$ K and for different χ values (full lines). Dashed lines are the VMSD given by Eq. (31).

that region is typically about one or two lattice parameters. Finally, the VMSD decreases and converges to zero.

Let the propagation length $L_p=\sqrt{2\ln(2)\langle x_0^2\rangle}$, where $\langle x_0^2\rangle$ is the maximum value of the VMSD, define the size of the region explored by the polaron. Its temperature dependence is illustrated in Fig. 6 for different χ values. The propagation length decreases with both χ and T. Nevertheless, at low temperature, L_p is almost χ independent since it varies from 3.14 for $\chi=30$ pN to 3.06 for $\chi=60$ pN at $T=10$ K. The deposited energy thus covers about three sites on each side of the excited site before being absorbed by the thermal bath. At biological temperature, the propagation length is strongly reduced and it is more sensitive to the coupling strength. It ranges between 1.17 for $\chi=30$ pN and 0.75 for $\chi=60$ pN.

The temperature dependence of both the dephasing constant Γ^* and the incoherent diffusion coefficient $D_i=\Gamma_0^+$ is shown in Figs. 7(a) and 7(b), respectively. Both parameters strongly depend on the temperature and they tend to zero as the temperature vanishes. At low temperature, the χ dependence of the parameters is rather small. The dephasing constant scales as T^2, whereas D_i increases linearly with T. By contrast, at high temperature, the χ dependence is more pronounced and two regimes occur. For small χ values, both Γ^* and D_i still increase with T. However, for large χ values, D_i reaches a maximum value at a critical temperature to finally

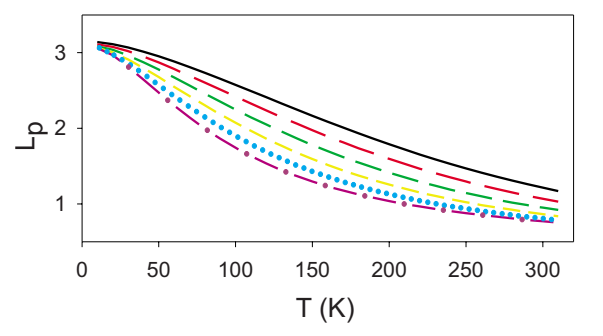

FIG. 6. (Color online) L_p vs T for $\chi=30$ pN (full line), $\chi=36$ pN (long dashed line), $\chi=42$ pN (medium dashed line), $\chi=48$ pN (short dashed line), $\chi=54$ pN (dotted line), and $\chi=60$ pN (dashed dotted line).

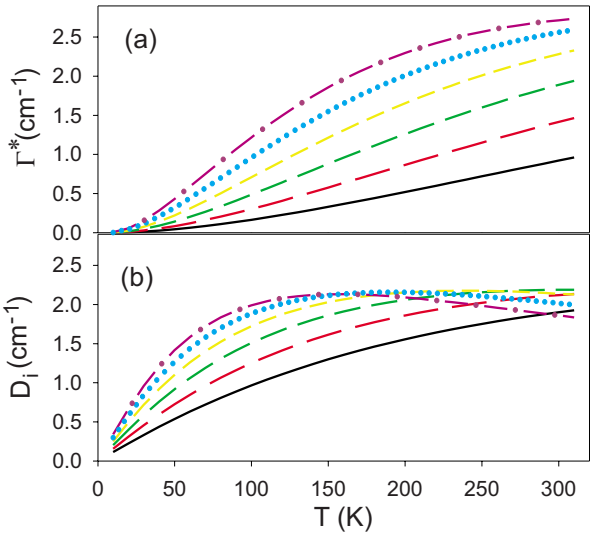

FIG. 7. (Color online) (a) Dephasing constant and (b) incoherent diffusion coefficient vs T for $\chi=30$ pN (full line), $\chi=36$ pN (long dashed line), $\chi=42$ pN (medium dashed line), $\chi=48$ pN (short dashed line), $\chi=54$ pN (dotted line), and $\chi=60$ pN (dashed dotted line).

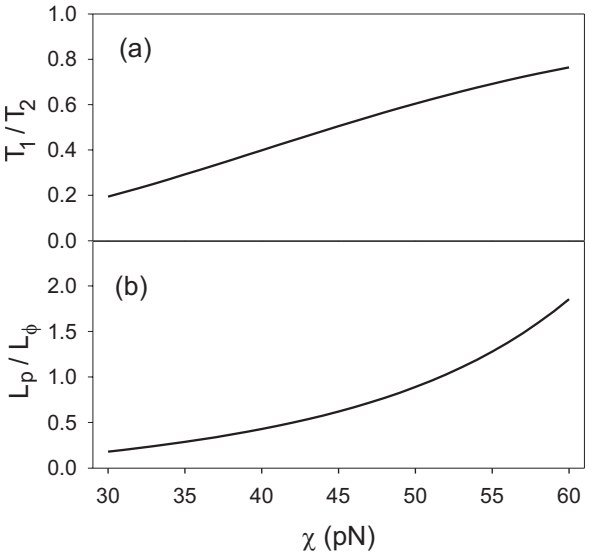

FIG. 8. χ dependence of (a) T_1/T_2 and (b) L_p/L_Φ for $T=310$ K.

decrease with T. The critical temperature decreases when χ increases. Similarly, although Γ^* does not reach a maximum on the range displayed in Fig. 7, a slowdown in its increase takes place. Note that the T dependence of Γ^* governs the behavior of the coherent diffusion coefficient $D_c=2\hat{\Phi}^2/\Gamma^*$ (not drawn in Fig. 7). We have verified that D_c decreases with both T and χ by exhibiting a divergence when T tends to zero.

Finally the χ dependence of the relevant parameters that control the transport properties is displayed in Fig. 8 for $T=310$ K. As shown in Fig. 8(a), the ratio between the lifetime and the dephasing time increases almost linearly with χ. It extends from 0.19 for $\chi=30$ pN to 0.76 for $\chi=60$ pN mainly due to the strong χ dependence of the dephasing constant [Fig. 7(a)]. Similarly, Fig. 8(b) displays the ratio L_p/L_ϕ where the coherent length $L_\phi=\sqrt{2}\hat{\Phi}/\Gamma^*$ defines the length covered coherently by the polaron. A critical value $\chi^* \approx 52$ pN discriminates between two situations since L_p is shorter than L_ϕ when $\chi<\chi^*$, whereas the opposite situation occurs when $\chi>\chi^*$. Note that the χ dependence of both the incoherent and the coherent diffusion coefficients has been studied numerically (not drawn in Fig. 8). The behavior of D_i results from the competition between the dressing mechanism, which prevents the polaron delocalization, and the effective hopping constant fluctuations. Therefore, it increases for small χ values to reach a maximum whose value is about $D_i=2.19$ cm^{-1} for $\chi=41$ pN. By contrast, since Γ^* increases with χ, the coherent diffusion coefficient rapidly decreases with the coupling strength. It varies from 40 cm^{-1} for $\chi=30$ pN to 0.45 cm^{-1} for $\chi=60$ pN. Consequently, in the strong-coupling limit, both D_i and D_c contribute significantly to the full diffusion coefficient. For instance, $D_i \approx D_c \approx 2.0$ cm^{-1} for $\chi=50$ pN.

VI. DISCUSSION

The numerical results clearly show that the vibron decay over the bath of intramolecular normal modes strongly modifies the transport properties. To discuss and interpret these features, let first focus our attention on the physics involved in the vibron annihilation. Indeed, the complexity of the vibron relaxation mainly results from the strong vibron-phonon coupling which discriminates between two kinds of eigenstates. When amide-I modes occupy their ground state, the phonons are described by standard number states. By contrast, when a vibron is created, each phonon mode experiences a linear perturbation so that its eigenstate becomes a superimposition of number states. Such superimpositions have a local meaning and they induce a lattice distortion responsible for the dressing of the vibron. Consequently, due to Fermi resonances, the bath absorbs the energy released by the vibron annihilation. During this annihilation, each phonon mode realizes a transition between a superimposition of number states and well-defined number states. These transitions give rise to fluctuations in the phonon number which accompanies the energy exchange between the amide-I modes and the thermal bath.

According to the standard time-dependent perturbation theory, the decay rate $\gamma_0(t)$ measures the system memory at time t of an initial vibron annihilation. As discussed in Sec. III, this memory is characterized by the full correlation function $f_B(t)C(t)$. For a sufficiently wide Fermi resonance, $f_B(t)$ decays over a time scale shorter than the phonon correlation time τ_c so that the dressing operator correlation function scales as $C(t) \approx \exp(-E_B kTt^2 - iE_B t)$. Therefore, $f_B(t)C(t)$ decreases according to a Gaussian law whose correlation time $\tau^*=(\alpha^2+E_B kT)^{-0.5}$ is very short when compared with the time $\hat{\Phi}^{-1}$ required for the polaron to leave the excited site. For instance, for $\chi=45$ pN, $\tau^*=0.08$ ps, whereas $\hat{\Phi}^{-1}=2.5$ ps. As a result, the relaxation occurs as if the polaron was immobile and the corresponding decay rate $\gamma_0(t)$ rapidly

increases to reach a constant value defined as [51]

$$\gamma_0 = \frac{G(T)}{\sqrt{\pi(\alpha^2 + E_B kT)}}. \tag{33}$$

As observed in Fig. 1, the corresponding lifetime increases with χ ($E_B \propto \chi^2$) and it decreases with the temperature. This equation gives a lifetime value in a rather good agreement with our numerical calculations provided that the temperature is sufficiently high. In particular, for $T=310$ K, the theoretical lifetime $T_1=1.23$ ps is very close to the numerical value equal to 1.24 ps for $\chi=45$ pN.

In that context, energy relaxation occurring over a very short time scale, it prevents any significant delocalization of the polaron along the lattice. At biological temperature, our numerical results have clearly shown that the polaron explores a finite region around the excited site whose size is typically about one or two lattice parameters. Nevertheless, although the vibron density localizes, the way the energy spreads out before the polaron relaxes strongly depends on the strength of the vibron-phonon interaction. Indeed, a transition between coherent and incoherent energy transfer takes place for a coupling strength typically about $\chi=50$ pN.

For a weak vibron-phonon coupling, the dephasing time is larger than the polaron lifetime so that the only source of dissipation involves the polaron relaxation over the bath of intramolecular normal modes. Consequently, the energy delocalizes coherently along the lattice until the polaron disappears which results in a propagation length shorter than the coherent length. The polaron eigenstates are thus Bloch wave with a well-defined wave vector K and with a complex energy $\omega_K=\omega_0-E_B+2\hat{\Phi}\cos(K)-i\gamma_0/2$. The polaron propagator corresponds to the free propagator (A1) times a damping term which arises from the finite lifetime. The resulting vibron density is thus written as

$$P(x,t) \approx |J_x(2\hat{\Phi}t)|^2 e^{-\gamma_0 t}. \tag{34}$$

When $\gamma_0=0$, Eq. (34) describes a purely coherent regime. For a given x value, $P(x,t)$ shows a main peak followed by small amplitude oscillations. The main peak occurs at time $t_0(x) \approx |x|/2\hat{\Phi}$ and its amplitude exhibits an algebraic decay as $P_0(x) \approx |x|^{-0.66}$. This slowly varying decay results from the lattice dispersion which is responsible for the spread out of the initial polaron wave packet which delocalizes with the standard group velocity.

When the polaron has a finite lifetime, Eq. (34) reveals a fully different behavior. Indeed, the damping term prevents the occurrence of the small amplitude oscillations so that the time evolution of $P(x,t)$ reduces to a bell-shaped peak very similar to the peak represented in Fig. 2 for $\chi=30$ pN. The peak amplitude does not decay algebraically any more but it decreases with site position according to an exponential law $P_0(x) \approx \exp(-x/\xi)$ once $x=4-5$. Note that as illustrated by the dotted line in Fig. 3(a), the curve $P_0(x)$ vs x provided by Eq. (34) clearly reproduces the behavior of the peak amplitude obtained from the numerical simulation of the GME (full line). In addition, $t_0(x)$ still increases almost linearly with x but the corresponding energy flow velocity is clearly enhanced by γ_0.

An analytical expression of both the localization length ξ and the energy flow velocity v_p can be extracted from the knowledge of the polaron Green function $G(\omega)=(\omega-H_{\mathrm{po}})^{-1}$. According to standard calculations [57], the Green function matrix elements are defined as

$$G_{x\bar{x}}(\omega) = -\frac{e^{-iK|x-\bar{x}|}}{2i\hat{\Phi}\sin(k)}, \tag{35}$$

where the wave vector $K \equiv K(\omega)$ is the solution of the equation $\omega=\omega_K$. Since ω_K is complex, $G_{x\bar{x}}(\omega)$ exhibits a localized nature characterized by the imaginary part of K. In addition, it is well known that the density of states given by the imaginary part of $G_{xx}(\omega)$ is inversely proportional to the group velocity. Considering an excitation whose frequency is located at the center of the band, these features allow to define the localization length as

$$\xi \approx \frac{1}{2\ln[(\gamma_0/4\hat{\Phi}) + \sqrt{1+(\gamma_0/4\hat{\Phi})^2}]}. \tag{36}$$

Similarly, the energy flow velocity is written as

$$v_p \approx 2\hat{\Phi}\sqrt{1+(\gamma_0/4\hat{\Phi})^2}. \tag{37}$$

These last two expressions give results in a rather good agreement with the numerical observations. For instance, for $\chi=30$ pN and $T=310$ K, they yield $\xi=1.80$ and $v_p=1.04v_g$ whereas the corresponding numerical values were $\xi=1.44$ and $v_p=1.10v_g$. Therefore, the finite lifetime is responsible for the localization of the vibron density according to a localization length which shows a logarithmic divergence with γ_0. In addition, it leads to an increase of the energy flow velocity which becomes slightly greater than the polaron group velocity. Note that for $\chi=30$ pN, $\gamma_0 \ll 4\hat{\Phi}$ so that $\xi \approx 2\hat{\Phi}T_1$. The localization length is thus equal to the distance covered coherently by the polaron during its lifetime.

In that context, the VMSD reduces to

$$\langle x^2(t)\rangle = 2\hat{\Phi}^2 t^2 e^{-\gamma_0 t}. \tag{38}$$

It scales as t^2 in the short time limit, as expected from standard transport theories. Nevertheless, it increases until it reaches a maximum at time $t=2T_1$. The value of this maximum yields the analytical expression of the propagation length as $L_p \approx 1.22\hat{\Phi}T_1$. The propagation length is thus about half the localization length ($L_p \approx 0.6\xi$). As illustrated in Fig. 9 (dotted line), this expression of L_p is in a close agreement with the corresponding numerical value (full line) provided that χ is sufficiently small. Note that $L_\phi/L_p \approx T_2/T_1 \gg 1$ in the weak-coupling limit.

For a strong vibron-phonon coupling, the dephasing time is shorter than or about to the polaron lifetime. Consequently, the diffusive regime is rapidly reached so that the energy delocalizes incoherently along the lattice until the polaron disappears. The propagation length is larger than the coherent length and the energy flow velocity is larger than the polaron group velocity. According to the standard diffusion theory, the long wavelength disturbance of the vibron density is governed by the Fick's law and it reduces to

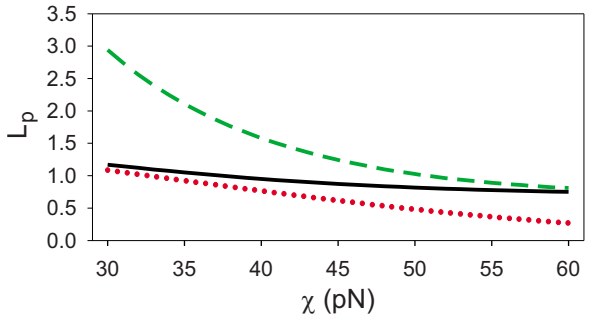

FIG. 9. (Color online) L_p vs χ (full line) for $T=310$ K. The dotted line and the dashed line represent L_p for the coherent regime and for the diffusive regime, respectively (see the text).

$$P(x,t) \approx \frac{e^{-\gamma_0 t}}{\sqrt{4\pi D t}} \exp\left(-\frac{x^2}{4Dt}\right), \tag{39}$$

where $D=D_i+D_c$. From Eq. (39), $P(x,t)$ describes the propagation of a rather asymmetric peak very similar to the peak represented in Fig. 2 for $\chi=60$ pN. This peak is maximum for $t_0(x) \approx |x|/\sqrt{4D\gamma_0}$ resulting in an energy flow velocity controlled by the diffusion coefficient as $v_p=2\sqrt{D/T_1}$. However, as in the coherent regime, the finite lifetime is responsible for a strong decrease of the peak amplitude with the site position. This amplitude exhibits an exponential decay $P_0(x)=\exp(-|x|/\xi)/\sqrt{2\pi\xi|x|}$ according to the localization length $\xi \approx \sqrt{DT_1}$. Note that for $\chi=60$ pN and $T=310$ K, Eq. (39) gives rise to $v_p=3.65v_g$ and $\xi=0.79$ which are very close to the numerical values equal to $v_p=4.01v_g$ and $\xi=0.77$, respectively. In addition, as shown in Fig. 3(c) (dashed line), the curve $P_0(x)$ vs x provided by Eq. (39) clearly reproduces the behavior of the peak amplitude obtained form the numerical calculations (full line).

In that context, the energy transport is clearly dominated by the incoherent propagation of the polaron. Although both the coherent and the incoherent diffusion coefficients contribute to the full diffusion coefficient, it is interesting to note that D_i predominates over D_c in the very strong-coupling limit (for $\chi=60$ pN, $D_i \approx 4D_c$). Nevertheless, as in the coherent regime, the finite lifetime favors the energy localization around the excited site. Consequently, the VMSD is expressed as

$$\langle x^2(t) \rangle = 2Dte^{-\gamma_0 t}. \tag{40}$$

It increases to reach a maximum value at time $t=T_1$. The propagation length, defined as $L_p \approx 1.01\sqrt{DT_1}$, represents the size of the region covered incoherently by the polaron before its disappearance in the bath of intramolecular normal modes. In the diffusive regime, $L_p \approx \xi$ and, as illustrated in Fig. 9 (dashed line), it is in a rather good agreement with the corresponding numerical value (full line) provided that χ is sufficiently large.

The transition between the coherent and the incoherent regime is intimately connected to the value of the dephasing constant $\Gamma^*=2[\Gamma_0^+-\Gamma_1^+]+[\Gamma_0^--\Gamma_1^-]$. Through the expression of the polaron-phonon correlation function [Eqs. (17) and (A4)], Γ^* generalizes the so-called γ_1 contribution of the Grover-Silbey approach [17] and it strongly depends on whether the phonon bath exhibits spatial correlations or not. Indeed, when the spatial correlations are disregarded, only $C_\pm(0,t)$ contributes significantly to the decay rates $\Gamma_m^\pm$ so that $\Gamma_0^\pm$ predominates over $\Gamma_1^\pm$ which almost vanishes. As a result, Γ^* is about 3.5 ± 0.5 cm^{-1} at biological temperature whatever the χ values. When the acoustic nature of the phonons is taken into account, $\Gamma_1^\pm$ turns on which reduces the dephasing constant. This effect is fundamental when the vibron-phonon coupling is sufficiently weak since Γ^* extends from 0.96 cm^{-1} with spatial correlations to 3.02 cm^{-1} without spatial correlations, for $\chi=30$ pN and $T=310$ K. The corresponding dephasing time thus reduces from $T_2=5.52$ ps to $T_2=1.75$ ps. In other words, spatial correlations in the phonon bath prevent the decoherence of the polaron and they allow the observation of the coherent regime during the polaron lifetime. Nevertheless, in the strong vibron-phonon coupling limit, the influence of the spatial correlations is less important resulting in a shorter dephasing time giving rise to the diffusive regime.

Finally, let us mention that the previous discussion shows the occurrence of two distinct regimes depending on whether the vibron-phonon interaction is weak or strong. However, the transition between these two regimes is not well-defined and the numerical results reveal that an intermediate regime takes place for intermediate values of the coupling. This feature is illustrated in Figs. 3(b) and 9 where neither the coherent regime nor the diffusive regime clearly reproduce the real behavior when $\chi \approx 45$ pN.

VII. CONCLUSION

In the present paper, a modified Davydov model has been used to describe the vibrational energy flow mediated by an amide-I vibron in a 1D lattice of H-bonded peptide units. Special attention has been paid to characterize the influence of the vibron energy relaxation on the transport properties. To proceed, the energy relaxation has been modeled by assuming that each amide-I mode interacts with a bath of intramolecular normal modes whose displacements are strongly localized on the C=O groups. Moreover, the dynamics has been addressed within the small polaron point of view to account on the strong coupling between the vibron and the phonons associated to the external motions of the peptide units.

Within the standard projector technique of the TCL approach, the GME for the polaron RDM has been simplified by using relevant approximations. It has been shown that the evolution of the RDM is governed by an effective Liouvillian with specific translational invariances. A Bloch transformation has been performed to finally obtain a GME isomorphic to the Schrödinger equation of a 1D lattice.

In that context, it has been shown that the energy relaxation occurs over a very short time scale resulting in a polaron lifetime of about 1.5 ps in a rather good agreement with experimental data. This finite lifetime prevents any significant delocalization of the polaron along the lattice. At biological temperature, the polaron explores a finite region around the excited site whose size is typically about one or

two lattice parameters. Nevertheless, the way the energy spreads out before the polaron relaxes strongly depends on the strength of the vibron-phonon coupling. For weak coupling, the dephasing time is larger than the polaron lifetime so that the only source of dissipation involves the polaron relaxation over the bath of intramolecular normal modes. The energy propagates coherently along the lattice until the polaron disappears. The finite lifetime favors the localization of the energy density whose amplitude decreases exponentially. In a marked contrast, for a strong coupling, the dephasing time is shorter than or about to the polaron lifetime. A diffusive regime takes place and the polaron explores a finite size region incoherently before its disappearance in the bath. As in the coherent regime, such a behavior gives rise to an exponential decay of the vibron density.

To conclude, let us mention that these results suggest that the dipole-dipole coupling does not play a fundamental role to understand the vibron dynamics at biological temperature. More precisely, considering the lateral coupling between a few amide-I modes surrounding the excited side appears sufficient to accurately describe the vibrational energy redistribution. Such an approach legitimizes previous works in which the dipole-dipole couplings have been neglected [50,51]. In addition, it provides a simplified way to investigate the multiquanta dynamics whose main difficulty originates from the size of the Hilbert space which drastically increases with both the site number and the vibron number [7,8,10,25,26]. On the other hand, much attention must be paid to improve the model describing the amide-I decay to clearly identify the nature of the bath of intramolecular normal modes and to define the relevant relaxation pathways in a real α helix.

APPENDIX: PARAMETERS DEFINING THE RELAXATION OPERATOR

In this appendix, the expression of the different terms occurring in the definition of the time-dependent relaxation operators [Eq. (13)] are given for a lattice with translational invariance. Therefore, let first define the polaron propagator $G(t)=\exp(-iH_{\mathrm{po}}t)$. Its matrix element $G_{x_1,x_2}(t)$ only depends on $|x_2-x_1|$ and it is expressed in terms of the Bessel function of the first kind $J_n(z)$ as

$$G_{0,x}(t) = (-i)^{|x|} e^{-i(\omega_0 - E_B)t} J_{|x|}(2\hat{\Phi}t), \tag{A1}$$

where $x=x_2-x_1$. The polaron propagation is governed by the effective hopping constant $\hat{\Phi}=\Phi\exp[-\Sigma(T)]$, where $\Sigma(T)$ is defined in terms of the temperature-dependent factor $N_q=\coth(\beta\Omega_q/2)$ as

$$\Sigma(T) = \frac{4E_B}{N\Omega_c}\sum_q \left|\sin\left(\frac{q}{2}\right)\right| \cos^2\left(\frac{q}{2}\right) N_q. \tag{A2}$$

Similarly, the correlation function of the dressing operator is site independent. It is written as

$$C(t) = e^{-k(t)-is(t)}, \tag{A3}$$

where $k(t)$ and $s(t)$ are expressed as

$$k(t) = \frac{2E_B}{N\Omega_c}\sum_q N_q \frac{\cos^2\left(\frac{q}{2}\right)}{\left|\sin\left(\frac{q}{2}\right)\right|}[1-\cos(\Omega_q t)],$$

$$s(t) = \frac{2E_B}{N\Omega_c}\sum_q \frac{\cos^2\left(\frac{q}{2}\right)}{\left|\sin\left(\frac{q}{2}\right)\right|}\sin(\Omega_q t).$$

The polaron-phonon coupling correlation functions $C_{\pm}^{y,s}(x,t)$ do not depend on both y and s. They are simply denoted $C_{\pm}(x,t)$ and they are defined as

$$C_{\pm}(x,t) = \hat{\Phi}^2(e^{\pm[K(x,t)-iS(x,t)]}-1), \tag{A4}$$

where $K(x,t)$ and $S(x,t)$ are given by

$$K(x,t) = \frac{8E_B}{N\Omega_c}\sum_q N_q \left|\sin\left(\frac{q}{2}\right)\right| \cos^2\left(\frac{q}{2}\right)\cos(\Omega_q t - qx),$$

$$S(x,t) = \frac{8E_B}{N\Omega_c}\sum_q \left|\sin\left(\frac{q}{2}\right)\right| \cos^2\left(\frac{q}{2}\right)\sin(\Omega_q t - qx).$$

At biological temperature these last two equations reduce to

$$K(x,t) = \frac{16E_B kT}{N\Omega_c^2}\sum_q \cos^2\left(\frac{q}{2}\right)\cos(\Omega_q t - qx),$$

$$S(x,t) = -\frac{1}{2kT}\frac{\partial}{\partial t}K(x,t).$$

Note that within the Debye model, i.e., $\Omega_q \approx \Omega_c q/2$, it is straightforward to show that $K(0,t)$ is a peaked function centered at the origin $t=0$. Its amplitude is equal to $8E_B kT/\Omega_c^2$ and its width is about the phonon correlation time $\tau_c=2/\Omega_c$. By contrast, $K(x,t)$ defines a peak centered on the propagation time $\tau_p=2|x|/\Omega_c$ over a time scale of about $2\tau_c$ and whose amplitude is equal to $4E_B kT/\Omega_c^2$.

[1] A. S. Davydov and N. I. Kisluka, Phys. Status Solidi B **59**, 465 (1973); Zh. Eksp. Teor. Fiz. **71**, 1090 (1976) [Sov. Phys. JETP **44**, 571 (1976)].
[2] D. W. Brown and Z. Ivic, Phys. Rev. B **40**, 9876 (1989).
[3] D. W. Brown, K. Lindenberg, and X. Wang, in *Davydov's Soliton Revisited*, edited by P. L. Christiansen and A. C. Scott (Plenum, New York, 1990).
[4] Z. Ivic, D. Kapor, M. Skrinjar, and Z. Popovic, Phys. Rev. B **48**, 3721 (1993).
[5] Z. Ivic, D. Kostic, Z. Przulj, and D. Kapor, J. Phys.: Condens. Matter **9**, 413 (1997).
[6] J. Tekic, Z. Ivic, S. Zekovic, and Z. Przulj, Phys. Rev. E **60**, 821 (1999).
[7] V. Pouthier, Phys. Rev. E **68**, 021909 (2003).
[8] V. Pouthier and C. Falvo, Phys. Rev. E **69**, 041906 (2004).
[9] C. Falvo and V. Pouthier, J. Chem. Phys. **123**, 184709 (2005).
[10] C. Falvo and V. Pouthier, J. Chem. Phys. **123**, 184710 (2005).
[11] D. V. Tsivlin and V. May, J. Chem. Phys. **125**, 224902 (2006).
[12] D. V. Tsivlin, H. Meyer, and V. May, J. Chem. Phys. **124**, 134907 (2006).
[13] J. Edler, R. Pfister, V. Pouthier, C. Falvo, and P. Hamm, Phys. Rev. Lett. **93**, 106405 (2004).
[14] J. Edler, V. Pouthier, C. Falvo, R. Pfister, and P. Hamm, in *Ultrafast Phenomena XIV*, edited by T. Kobayashi, T. Okada, T. Kobayashi, K. Nelson, and S. De Silvesti, Vol. 79 of Springer Series in Chemical Physics (Springer, Berlin, 2005).
[15] I. G. Lang and Yu. A. Firsov, Sov. Phys. JETP **16**, 1293 (1962).
[16] V. M. Kenkre and P. Reineker, *Exciton Dynamics in Molecular Crystals and Aggregates* (Springer, Berlin, 1982).
[17] M. Grover and R. Silbey, J. Chem. Phys. **54**, 4843 (1971).
[18] R. Silbey and R. W. Munn, J. Chem. Phys. **72**, 2763 (1980).
[19] R. W. Munn and R. Silbey, J. Chem. Phys. **83**, 1843 (1985).
[20] R. W. Munn and R. Silbey, J. Chem. Phys. **83**, 1854 (1985).
[21] V. Capek and I. Barvik, J. Phys. C **20**, 1459 (1987).
[22] B. J. West and K. Lindenberg, J. Chem. Phys. **83**, 4118 (1985).
[23] D. Brown, K. Lindenberg, and B. J. West, J. Chem. Phys. **83**, 4136 (1985).
[24] H. Dolderer and M. Wagner, J. Chem. Phys. **108**, 261 (1998).
[25] V. Pouthier, Physica D **221**, 13 (2006).
[26] V. Pouthier, Physica D **237**, 106 (2008).
[27] R. Zwanzig, in *Lectures in Theoretical Physics*, edited by W. E. Brittin, B. W. Downs, and J. Downs (Interscience Publishers, Inc., New York, 1961), Vol. III, pp. 106–141; Physica (Amsterdam) **30**, 1109 (1964); J. Chem. Phys. **33**, 1338 (1960).
[28] H. Mori, Prog. Theor. Phys. **33**, 423 (1965); **34**, 399 (1965).
[29] V. May and O. Kuhn, *Charge and Energy Transfer Dynamics in Molecular Systems* (Wiley-VCH Verlag, Berlin, 2000).
[30] K. A. Peterson, C. W. Rella, J. R. Engholm, and H. H. Schwettman, J. Phys. Chem. B **103**, 557 (1999).
[31] R. H. Austin, A. Xie, L. Van der Meer, M. Shinn, and G. Neil, Nucl. Instrum. Methods Phys. Res. A **507**, 561 (2003).
[32] A. Xie, L. van der Meer, W. Hoff, and R. H. Austin, Phys. Rev. Lett. **84**, 5435 (2000).
[33] P. Hamm, M. Lim, and R. M. Hochstrasser, J. Phys. Chem. B **102**, 6123 (1998).
[34] P. Hamm, M. Lim, W. F. DeGrado, and R. M. Hochstrasser, J. Chem. Phys. **112**, 1907 (2000).
[35] S. Woutersen and P. Hamm, J. Chem. Phys. **115**, 7737 (2001).
[36] J. Edler and P. Hamm, J. Chem. Phys. **117**, 2415 (2002).
[37] M. F. DeCamp, L. DeFlores, J. M. MacCracken, A. Tokmakoff, K. Kwac, and M. Cho, J. Phys. Chem. B **109**, 11016 (2005).
[38] K. Moritsugu, O. Miyashita, and A. Kidera, Phys. Rev. Lett. **85**, 3970 (2000).
[39] H. Fujisaki, Y. Zhang, and J. E. Straub, J. Chem. Phys. **124**, 144910 (2006).
[40] F. Shibata, Y. Takahashi, and N. Hashitsume, J. Stat. Phys. **17**, 171 (1977).
[41] C. Uchiyama and F. Shibata, Phys. Rev. E **60**, 2636 (1999).
[42] H. P. Breuer, B. Kappler, and F. Petruccione, Ann. Phys. **291**, 36 (2001).
[43] H. P. Breuer, B. Kappler, and F. Petruccione, Phys. Rev. A **59**, 1633 (1999).
[44] H. P. Breuer, J. Gemmer, and M. Michel, Phys. Rev. E **73**, 016139 (2006).
[45] M. Schroder, U. Kleinekathofer, and M. Schreiber, J. Chem. Phys. **124**, 084903 (2006).
[46] A. Pereverzev and E. Bittner, J. Chem. Phys. **125**, 104906 (2006).
[47] V. Pouthier, Phys. Rev. E **75**, 061910 (2007).
[48] P. A. S. Silva and L. Cruzeiro, Phys. Rev. E **74**, 021920 (2006).
[49] P. A. S. Silva and L. Cruzeiro-Hansson, Phys. Lett. A **315** (6), 447 (2003).
[50] V. Pouthier, J. Chem. Phys. **128**, 065101 (2008).
[51] V. Pouthier and Y. O. Tsybin, J. Chem. Phys. **129**, 095106 (2008).
[52] N. G. Mirkin and S. Krimm, J. Mol. Struct. **377**, 219 (1996).
[53] P. Derreumaux and G. Veroten, J. Chem. Phys. **102**, 8586 (1995).
[54] S. H. Lee and S. Krimm, Chem. Phys. **230**, 277 (1998).
[55] T. Holstein, Ann. Phys. (N.Y.) **8**, 343 (1959); E. I. Rashba, in *Excitons*, edited by E. I. Rashba and M. Struge (North-Holland, Amsterdam, 1982).
[56] M. Esposito and P. Gaspard, Phys. Rev. B **71**, 214302 (2005).
[57] L. Dobrzynski, Surf. Sci. **299-300**, 1008 (1994).